

Analytical and experimental study on the second harmonic mode response of a bulk acoustic wave resonator

This content has been downloaded from IOPscience. Please scroll down to see the full text.

2010 J. Micromech. Microeng. 20 115015

(<http://iopscience.iop.org/0960-1317/20/11/115015>)

View [the table of contents for this issue](#), or go to the [journal homepage](#) for more

Download details:

IP Address: 149.169.115.242

This content was downloaded on 09/02/2015 at 03:49

Please note that [terms and conditions apply](#).

Analytical and experimental study on the second harmonic mode response of a bulk acoustic wave resonator

Wei Pang¹, Hao Zhang¹, Richard C Ruby², Hongyu Yu³ and Eun Sok Kim⁴

¹ College of Precision Instrument and Opto-Electronics Engineering, Tianjin University, Tianjin 300072, People's Republic of China

² Avago Technologies, Inc., San Jose, CA 95131, USA

³ School of Earth and Space Exploration, Arizona State University, Tempe, Arizona 85287, USA

⁴ Department of Electrical Engineering, University of Southern California, Los Angeles, CA 90089, USA

E-mail: haozhang@tju.edu.cn

Received 9 July 2010, in final form 6 September 2010

Published 15 October 2010

Online at stacks.iop.org/JMM/20/115015

Abstract

A one-dimensional Mason model is employed to investigate the second harmonic mode response of a multilayer composite film bulk acoustic resonator (FBAR), particularly the dependence of the effective coupling coefficient ($K_{t,\text{eff}}^2$) on material properties and relative position in the acoustic stack. The simulation results for AlN-based FBAR with electrode layer having relatively low acoustic impedance and additional temperature compensation layer reveals that the maximum values of $K_{t,\text{eff}}^2$ are obtained with a thickness ratio (between the non-piezoelectric layer and piezoelectric layer) that is close to its acoustic velocity ratio. The fundamental mode and second harmonic mode operation of an FBAR are compared. The maximum achievable $K_{t,\text{eff}}^2$ is comparable (5.39% versus 5.16%) for the temperature compensated FBAR (with Mo as electrodes) operating at fundamental and second harmonic modes. However, the trimming-mass and crossover temperature sensitivities of the second harmonic mode are lower, indicating its potential advantage over the fundamental mode for high frequency applications above 2 GHz (such as filters, low phase noise temperature stable oscillator applications). Experimental results on a ZnO-based FBAR (Al/ZnO/Al/Si_xN_y) operating around 5 GHz with various thicknesses of ZnO and Si_xN_y show good agreement with numerical modeling.

(Some figures in this article are in colour only in the electronic version)

1. Introduction

The simplest configuration of a film bulk acoustic resonator (FBAR) is a thin film of piezoelectric material sandwiched between two metals with equal thickness [1]. When an ac electrical power is applied to the electrodes, a time-varying electric field is generated within the piezoelectric film along its thickness direction, and a longitudinal acoustic wave is excited in the film, propagating along the electric field direction. The wave is reflected at the electrode/air interfaces because of the impedance mismatch, and forms a standing wave, if the frequency of the ac signal is equal to an integer multiple

(n) of the fundamental resonant frequency (f_0), which is determined by the material properties (e.g., acoustic velocity) and thickness of composed layers in the resonator stack. In the case of the simplest FBAR composed of metal/piezoelectric film/metal with symmetric top and bottom metals, there are only odd harmonics (i.e. only odd n), because of the fact that the net strain across the thickness direction is zero in the case of even harmonics.

The electrode's surface smoothness and material properties including its sheet resistance, acoustic impedance and acoustic loss are of great importance to the FBAR's performance. In addition, the bottom electrode is especially

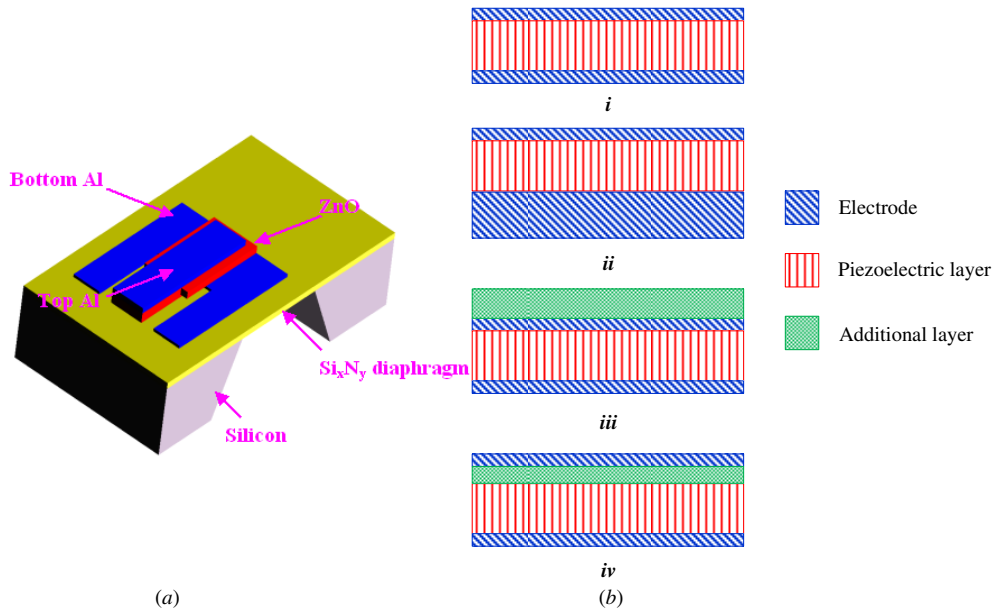


Figure 1. (a) Schematics of a bulk micromachined FBAR and (b) one symmetric and three non-symmetric configurations of the piezoelectric layer and non-piezoelectric layers for the FBAR.

critical, since it affects the piezoelectric film growth. High acoustic impedance materials, such as tungsten (W) and molybdenum (Mo) having reasonable conductivity, are commonly used for FBAR electrodes, while the thickness ratio between the piezoelectric layer and the electrode is selected to optimize the effective coupling coefficient $K_{r,\text{eff}}^2$ and Q factor for RF front-end filters. It was reported that the state-of-the-art FBARs (made of symmetric metal/AlN/metal similar to case (i) of figure 1(b)) exhibited a higher $K_{r,\text{eff}}^2$ and Q with thicker metals because of its relatively low acoustic loss [2]. It is noted that ‘hard’ materials with high acoustic velocity typically have lower acoustic loss.

If an FBAR is composed of non-symmetric metals (e.g. thin metal/piezoelectric layer/thick metal) or with an additional layer (e.g. metal/piezoelectric layer/metal/SiO₂) as shown in case (ii), case (iii) and case (iv) of figure 1(b), there are even harmonics in addition to odd harmonics because of the non-symmetric acoustic energy distribution along the thickness direction of the piezoelectric layer. The additional layer is typically dielectrics, and may be used to enhance the resonator’s functionality such as passivation, temperature compensation, mechanical reliability (for membrane-type, free-standing resonators), etc. If the dielectric layer (e.g. SiO₂) is arranged between the electrodes of the resonator, it acts as a series capacitance that greatly reduces the $K_{r,\text{eff}}^2$ of the resonator. In the analysis we performed below, we assume the dielectric layer could be ‘shorted’ and the entire voltage drop would be in the piezoelectric layer.

Most oscillator applications require the FBAR’s resonant frequency to fall within 0.01% of a target value. Accordingly, if no trimming is used, the thickness, acoustic velocity and density of each layer in the device will have to be controlled in a similar way. It is extremely difficult to yield thickness uniformity within such a tight tolerance over a wafer and from

wafer to wafer. As a consequence, frequency trimming is one of the key processes in FBAR manufacturing.

As the FBAR’s application areas grow to include frequencies beyond 10 GHz for microwave and wireless communication systems [3, 4], in order to operate the FBAR at its fundamental mode beyond 10 GHz, the thicknesses of piezoelectric and electrode films have to be thinned down to a level where precise control of the film quality (piezoelectric properties, series resistance, orientation, stress, etc) and thickness uniformity becomes very difficult. The electrical (ohmic) loss due to the finite conductivity of the ultrathin (~10 nm) electrodes greatly degrades the quality factor at the series resonance of a resonator, since its electrical impedance at this point is low and the series resistance becomes fairly large. Another challenge in using the fundamental mode is in correcting the thickness non-uniformity that requires localized film thickness trimming in the sub-angstrom accuracy. In contrast, the second harmonic mode operation naturally renders a higher frequency for a given film thickness and alleviates the trimming processing requirement. Consequently, operating an FBAR at its second harmonic mode frequency can extend the FBAR operation frequency range, as long as its figure of merit (FOM) remains high. With the non-symmetric FBAR structure, one can use a low acoustic-loss support layer (such as single crystal silicon, lithium niobate, quartz, etc) to increase the FBAR’s overall Q factor. In addition, the area to the perimeter ratio is higher for the second harmonic mode resonator, which improves Q near f_p . Thicker metal electrodes keep Q high near f_s .

An FBAR-based mass sensor operating in vapor and liquid has emerged as an appealing platform for highly sensitive biological and chemical detection. Significant progress has been made to improve the sensor’s mass sensitivity, mass resolution and immunity to the change of environmental temperature by adding a temperature compensation layer (e.g.

Table 1. Material properties used in the simulation [2].

Material	Density (kg m ⁻³)	Acoustic velocity (m s ⁻¹)	Temperature coefficient of velocity (ppm °C ⁻¹)	Acoustic impedance (MRayls)	Acoustic attenuation			
					η ($\times 10^{-3}$)	α (dB cm ⁻¹) at 1 GHz	k_t^2 (%)	ϵ_r
ZnO	5675	6393	–	36.3	5	6	7.9	8.8
AlN	3260	11 050	–22.1	36	20	8	6.5	10.5
Mo	10 280	6 213	–37.5	63.8	7.2	5	–	–
Al	2700	6295	–	17	7	18	–	–
SiO ₂	2650	5500	+77	14.6	3.6	14	–	3.9
Si	2330	8430	–	19.6	5.5	6.8	–	–
Si _x N _y	3270	11 000	–	35.9	30	12	–	7.5

amorphous SiO₂ film) in the acoustic path of a resonator. Also, it was reported that an FBAR at the second harmonic mode showed a much higher Q factor than the one at the fundamental mode in liquid environment, though both FBARs operated at similar frequencies, and had comparable mass sensitivities [5], thus indicating better mass resolution for the second harmonic mode operation. Finally, while a temperature compensated FBAR at the fundamental mode has been analyzed [6], the effects of the temperature-compensation layer on the FBAR's second harmonic mode performance have not been investigated.

In this paper, we provide a comprehensive theoretical study of the mass sensitivity, electromechanical coupling and manufacturing tolerances of a temperature compensated, second harmonic mode FBAR, and present its advantages over the fundamental mode.

2. Simulation and theoretical analysis

2.1. Modeling and simulation method

For an FBAR with a four-layer structure (two metal layers, a piezoelectric layer and a dielectric layer as shown in case (ii), case (iii) and case (iv) of figure 1(b)), the input impedance Z_{in} can be expressed by the following equation [7]:

$$Z_{in} = \frac{1}{j\omega C_0} \left[1 - \frac{k_t^2}{\gamma} \frac{(Z_1 + Z_2) \sin \gamma + j2(1 - \cos \gamma)}{(Z_1 + Z_2) \cos \gamma + j(1 + Z_1 Z_2) \sin \gamma} \right], \quad (1)$$

where C_0 , k_t^2 , $\gamma \approx \omega l/V$ are the clamped plate capacitance, the electromechanical coupling coefficient of the piezoelectric film, the phase delay of the longitudinal acoustic wave with piezoelectrically stiffened velocity V in AlN (or ZnO), respectively. Z_1 and Z_2 are the acoustic loading impedances on both sides of AlN (or ZnO) layer normalized to $Z_0 = \rho V$, the acoustic impedance of AlN (or ZnO) with ρ being the AlN (or ZnO) mass density. The loss due to the series resistance of the electrode is included. The dielectric loss ($\tan \delta$) of the piezoelectric film is added as a series resistance R_0 next to the clamped static capacitor C_0 . In order to obtain an accurate model (mainly for Q factor calculation), the acoustic loss of each layer is accounted for by adding complex terms to the real material stiffness as $c = c^E + j2\pi f \eta$, where c , c^E and η are the complex stiffness, the stiffness at constant electric field and the acoustic viscosity, respectively.

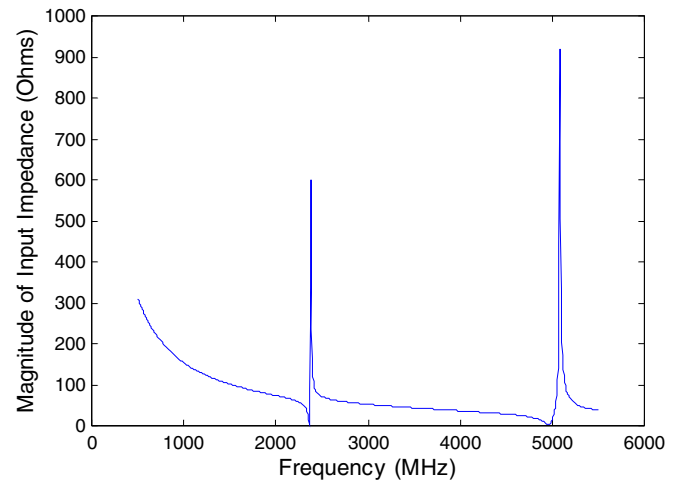


Figure 2. Simulated broadband input impedance of an FBAR consisting of Al/ZnO/Al/SiO₂.

We have done numerical analyses with the above equations to optimize the second harmonic mode resonance of the FBAR. Once we have obtained the input impedance spectra as a function of frequency, the series and parallel resonant frequencies (f_s and f_p , respectively) are obtained as the frequencies at which the magnitude of the impedance is the minimum and maximum, respectively. The effective electromechanical coupling coefficient $K_{t,\text{eff}}^2$ is derived as $(\pi^2/4) * f_s(f_p - f_s) / f_p^2$. Table 1 lists the various material parameters used in the simulation. Figure 2 shows the simulated broadband impedance of the FBAR consisting of Al/ZnO/Al/SiO₂. A second harmonic mode resonance is clearly shown beside the fundamental resonance. The second harmonic mode resonance occurs at a frequency approximately double that of the fundamental resonance.

As illustrated in figure 3, we keep the resonance frequency of the FBAR at 20 GHz (in the K band) and the passivation layer (i.e. SiO₂) on top of the upper electrode to be 300 Å thick. Then we vary the thickness ratio of the electrode (Al, Mo or W) to the piezoelectric layer (AlN) to obtain $K_{t,\text{eff}}^2$ for each ratio. Obviously, the electrode material with higher acoustic impedance renders higher maximum $K_{t,\text{eff}}^2$. When the maximum $K_{t,\text{eff}}^2$ is achieved, the exact thickness of each layer is calculated and listed in table 2. We see that both the piezoelectric and electrode films are very thin, and will require a very tight control on the film depositions.

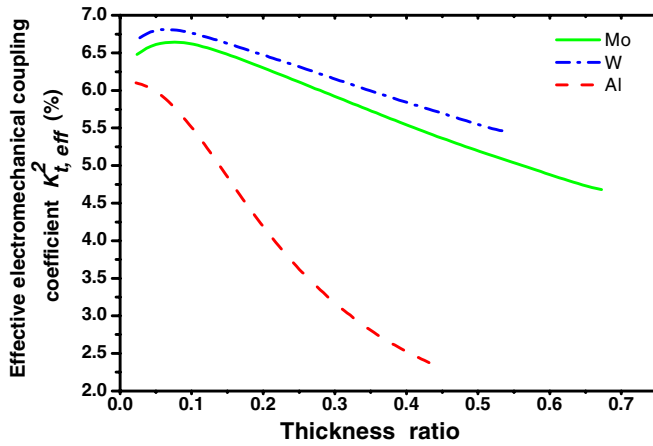


Figure 3. Simulated effective electromechanical coupling of the fundamental mode, 20 GHz FBAR (consisting of metal/AlN/metal/SiO₂), as a function of the thickness ratio of different metals (Al, Mo and W, respectively) to AlN. The metals have an equal thickness on both sides and 300 Å thick SiO₂ is selected as a passivation layer on top of the upper electrode.

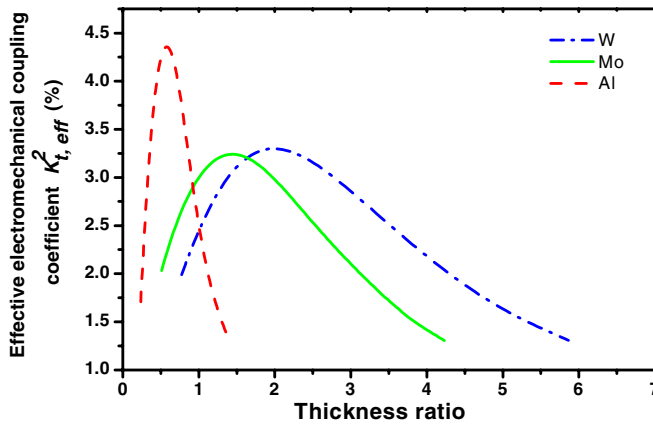


Figure 4. Simulated effective electromechanical coupling of the second harmonic mode, 20 GHz FBAR (consisting of thin metal/AlN/thick metal), as a function of the thickness ratio of different metals (Al, Mo and W, respectively) to AlN.

Table 2. Thickness (in Å) of each layer for a fundamental mode, 20 GHz FBAR with maximum $K_{t,eff}^2$.

Electrode	AlN	Electrode	SiO ₂
53 (Al)	2390	53 (Al)	300
135 (Mo)	1740	135 (Mo)	300
102 (W)	1510	102 (W)	300

2.2. Analysis of second harmonic mode response of two resonator structures

For second harmonic mode simulation, we consider two different structures shown in figure 1(b): a thin metal/piezoelectric layer/thick metal (case (ii)) and metal/piezoelectric layer/metal/SiO₂ (case (iii)). In the former case, we keep the thin electrode to be 200 Å, and then vary the thickness ratio of the thick electrode to the AlN layer to obtain the $K_{t,eff}^2$ curves. The three curves in figure 4 represent three different metals for the electrode and we can see how

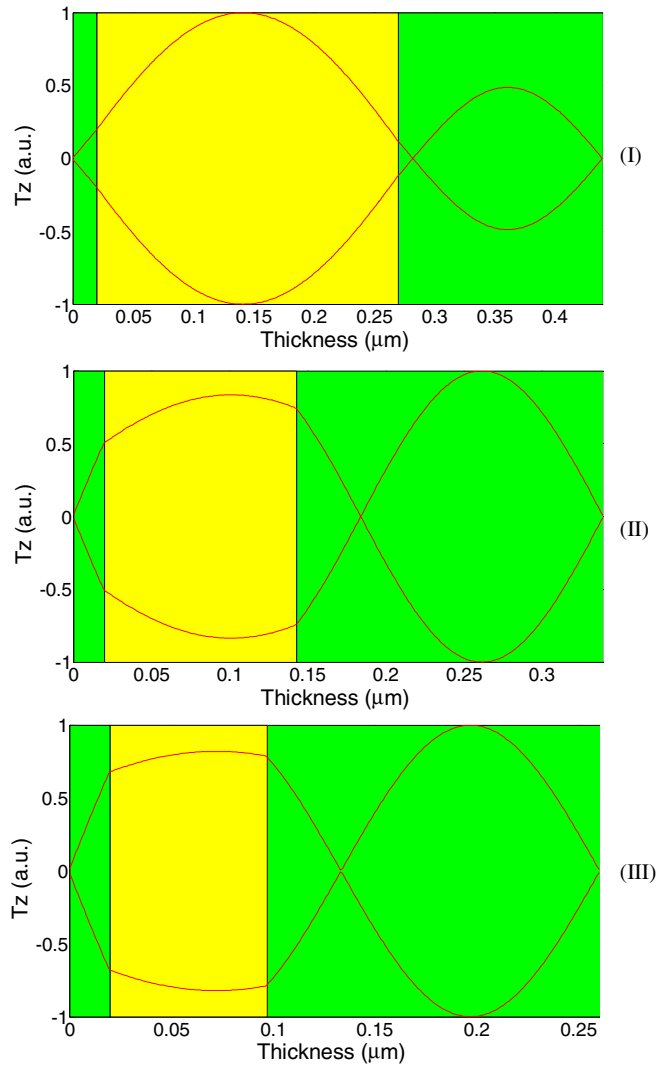


Figure 5. Calculated acoustic standing wave stress field of the second harmonic mode, 20 GHz FBAR consisting of thin metal/AlN/thick metal (from left to right), as a function of the depth into the resonator. (I), (II), (III) are for the Al, Mo, W electrode, respectively.

the effective coupling depends on the material properties of the electrodes. Most notably, unlike the fundamental mode case, the lower acoustic impedance electrodes increase the maximum achievable $K_{t,eff}^2$. The thickness ratio is larger when an electrode of higher acoustic impedance is used, which indicates that more of the resonator volume is occupied by a non-piezoelectric electrode material. Also, as can be seen in figure 5 which plots the associated stress field inside the resonator at the resonant frequency (i.e. 20 GHz) for the three electrode materials with maximum $K_{t,eff}^2$ achieved, the electrode of higher acoustic impedance produces a larger total stress in the electrode and a smaller portion of mechanical energy inside the piezoelectric layer, which to some extent explain why the maximum $K_{t,eff}^2$ is lower in this case.

For the structure shown in case (iii) of figure 1(b), SiO₂ is introduced for passivation and temperature compensation considerations as described in section 2.4. The electrode on each side of the piezoelectric film is 200 Å thick, and

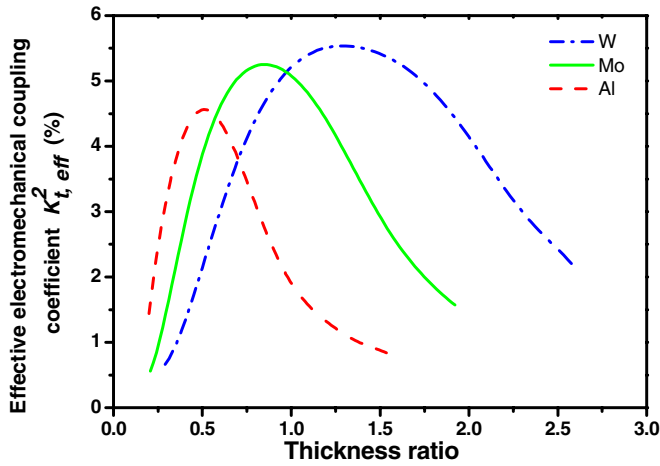


Figure 6. Simulated effective electromechanical coupling of the second harmonic mode, 20 GHz FBAR (consisting of metal/AlN/metal/SiO₂), as a function of the thickness ratio of SiO₂ to AlN. The thickness of each metal layer is equally fixed as 200 Å to have reasonably low sheet resistance.

has acceptable series resistance at 20 GHz. The simulated coupling coefficient versus the ratio of SiO₂ thickness to piezoelectric thickness is shown in figure 6. The remarkable trend is that the electrode with higher acoustic impedance has higher maximum $K_{t,eff}^2$, similar to the fundamental mode case. For example, the maximum $K_{t,eff}^2$ with tungsten electrode is about 5.5%, 20% higher than that ($K_{t,eff}^2 \sim 4.5\%$) with an aluminum electrode. This is understandable, since the electrode has a higher acoustic impedance than SiO₂, and behaves as an impedance mismatch layer to reflect acoustic energy into the piezoelectric layer. Another fact is that the stress distribution in the electrode/piezoelectric layer/electrode is almost identical to that of the fundamental mode when maximum $K_{t,eff}^2$ is achieved for each selected electrode material. The effects of high acoustic impedance electrodes can be qualitatively understood by looking at the stress distribution inside the composite structure shown in figure 7. The shape of the stress field matches the shape of the electric field better for the high impedance electrode case, resulting in an improved match in the distribution of acoustic standing wave to the linear distribution of the applied electric potential. This is brought about because of the discontinuity of the stress gradient at the piezoelectric-layer/electrode boundaries, caused by the acoustic impedance mismatch.

It is interesting to note that there exists an optimal thickness ratio in each case for a highest $K_{t,eff}^2$ and the crossover point in the stress curves is around the interface between the electrode layer and the SiO₂ layer. In case the electrode material (e.g. aluminum in figure 7(I)) has a relatively lower acoustic impedance than that of the piezoelectric layer, the highest $K_{t,eff}^2$ occurs at a thickness ratio that is close to the acoustic-velocity ratio between the piezoelectric layer to the SiO₂ layer, that is $\frac{l_{piezo}}{l_{sup}} \approx \frac{v_{piezo}}{v_{sup}}$. This is reasonable because that condition means that the largest acoustic standing wave is generated in both the piezoelectric layer and the support layer. The largest standing wave is possible because the wave in the

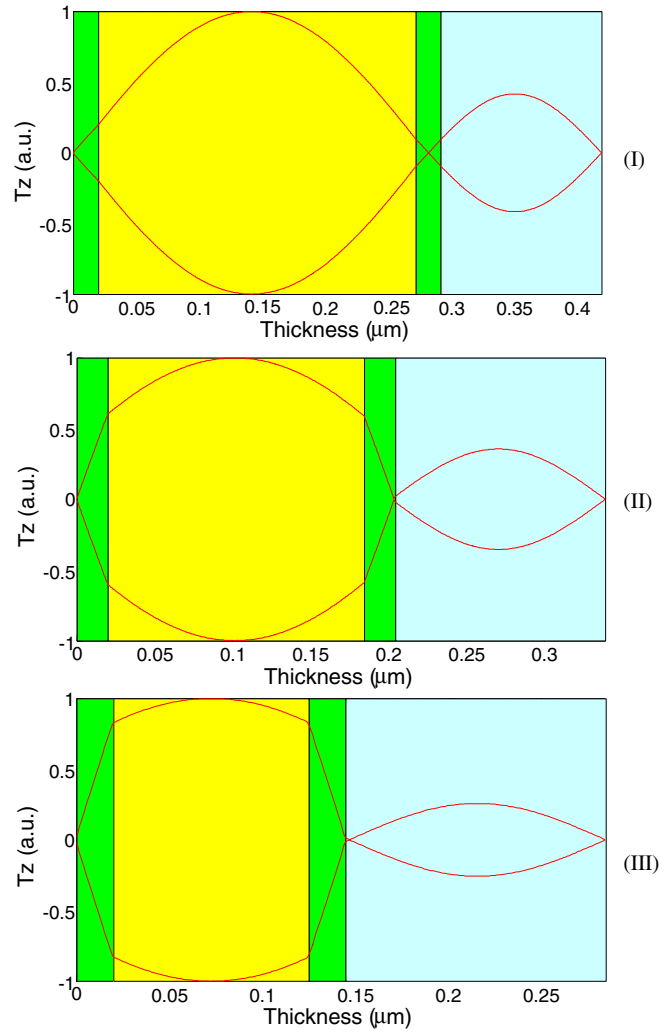


Figure 7. Calculated acoustic standing wave stress field of the second harmonic mode, 20 GHz FBAR consisting of metal/AlN/metal/SiO₂ (from left to right), as a function of the depth into the resonator. The thickness of each metal layer is equally fixed as 200 Å. (I), (II) and (III) are for the Al, Mo and W electrode, respectively.

support layer (through forward and backward propagation) experiences a 2π phase shift by the time it returns to the piezoelectric layer (that produces the wave due to an external excitation), and is in phase with the wave in the piezoelectric layer. In other words, the wave entering the piezoelectric layer from the support layer reinforces the resonance, resulting in the largest standing wave in both the piezoelectric and support layers, when the above condition is met. This is why the highest $K_{t,eff}^2$ can be achieved right at a specific thickness ratio between the piezoelectric and support layers.

2.3. Mass sensitivity comparison of the fundamental mode and second harmonic mode response

An FBAR device coated with a thin film of analyte-selective material on the wave propagation path can be used as a frequency control element in the feedback loop of an oscillator, which works as a bio/chemical sensor [8]. Mass added on the

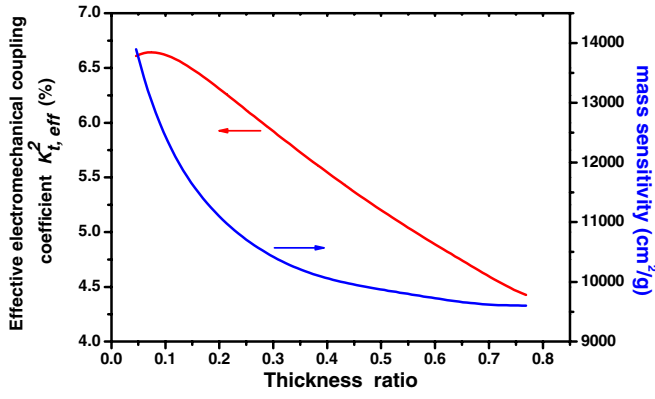


Figure 8. Simulated mass sensitivity and $K_{t,eff}^2$ of the fundamental mode, 20 GHz FBAR consisting of structure A: Mo/AlN/Mo/SiO₂, as a function of the thickness ratio of Mo to AlN. The thickness of SiO₂ is 300 Å.

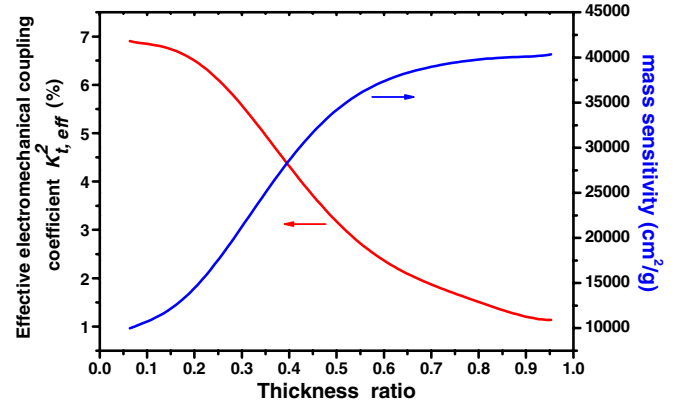


Figure 9. Simulated mass sensitivity and $K_{t,eff}^2$ of the fundamental mode, 20 GHz FBAR consisting of structure B: Mo/AlN/Mo/SiO₂, as a function of the thickness ratio of SiO₂ to AlN. The thickness of each Mo layer is selected as 130 Å to maximize $K_{t,eff}^2$.

surface of the FBAR causes a frequency shift (Δf) on the FBAR's resonant frequency. The mass sensitivity S can be calculated by the following equation [9, 10]:

$$S = \frac{\Delta f/f_0}{\rho_m t_m} = -\frac{(\pi f_0)^2 u_m^2}{E_{kin}^{total}} = -\frac{1}{2} \frac{u_m^2}{\sum_{i=1}^N \left(\int_0^{h_i} \rho_i u_i(z)^2 dz \right)}, \quad (2)$$

where $E_{kin}^{total} = 2(\pi f_0)^2 \int_{Layer_i} \rho_i u_i(z)^2 dz$ is the sum of kinetic acoustic energy in each layer; ρ_m and t_m are the density and thickness of the added mass layer, respectively; and u_m is the displacement of the added layer.

To make FBAR-based oscillators or sensors within the targeted frequency tolerance, post-fabrication frequency trimming is necessary to compensate film thickness variations. Either local etching or deposition on one (typically the uppermost passivation layer) or multiple layers, depending on accuracy requirements and throughput considerations, is used for the frequency trimming. The mass sensitivity for trimming is preferred to be low for the purpose of very accurate trimming, while a higher sensitivity is generally needed for sensing applications. This trade-off becomes much more demanding when the frequency is pushed upward beyond 10 GHz, because the sensitivity increases proportional to the resonance frequency.

The dependences of the mass sensitivity and electromechanical coupling on the thickness ratio of Mo and SiO₂ to AlN for the fundamental mode, 20 GHz FBARs, are shown in figures 8 and 9. The mass sensitivity for trimming and $K_{t,eff}^2$ is lower and higher, respectively, for structure A shown in figure 8 than structure B in figure 9. Thus, for oscillator or filter applications requiring stringent frequency accuracy, structure A is preferred, while for highly sensitive sensor applications where medium $K_{t,eff}^2$ is sufficient, structure B may be adopted. Nevertheless, there is a trade-off between the coupling coefficient and mass sensitivity for structure B.

With respect to the second harmonic mode response, similar analysis at 20 GHz is done with an eye on the effect of the SiO₂ layer on temperature compensation. Figure 10 shows plots of the mass sensitivity and $K_{t,eff}^2$ versus the thickness

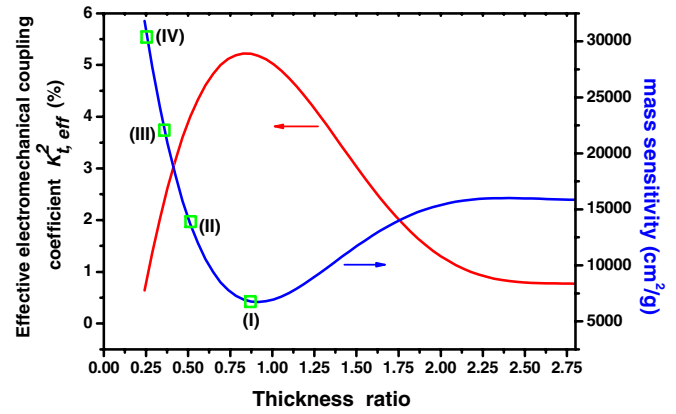


Figure 10. Simulated mass sensitivity and $K_{t,eff}^2$ of the second harmonic mode, 20 GHz FBAR consisting of Mo/AlN/Mo/SiO₂, as a function of the thickness ratio of SiO₂ to AlN. The thickness of each Mo layer is 200 Å.

ratio of SiO₂ to AlN. Similar to the fundamental mode for structure B, the coupling coefficient improves at the cost of the mass sensitivity. Coincidentally, when the maximum of $K_{t,eff}^2$ is achieved, the mass sensitivity reaches its minimum. For the same $K_{t,eff}^2$ ($\sim 5.25\%$), the trimming sensitivity value of $\sim 6780 \text{ cm}^2 \text{ g}^{-1}$ in figure 10 for the second harmonic mode is 31% lower than the fundamental one ($\sim 9880 \text{ cm}^2 \text{ g}^{-1}$) in figure 8.

From equation (2), we can see that the mass sensitivity depends on the density of each layer and displacement of the added layer normalized to the total acoustic energy inside the composite structure as well as the frequency. This is in accordance with our intuitive physical concept: when the multilayer mass sensor weighs less and the displacement amplitude at the sensing surface is larger, the added layer disturbs the resonant frequency more significantly, producing a higher mass sensitivity. Figure 11 plots the relative displacement versus depth for each of the four points (I, II, III and IV) on the mass sensitivity curve in figure 10, showing that the relative displacement in the added layer (on the right-hand side) is correlated with the sensitivity.

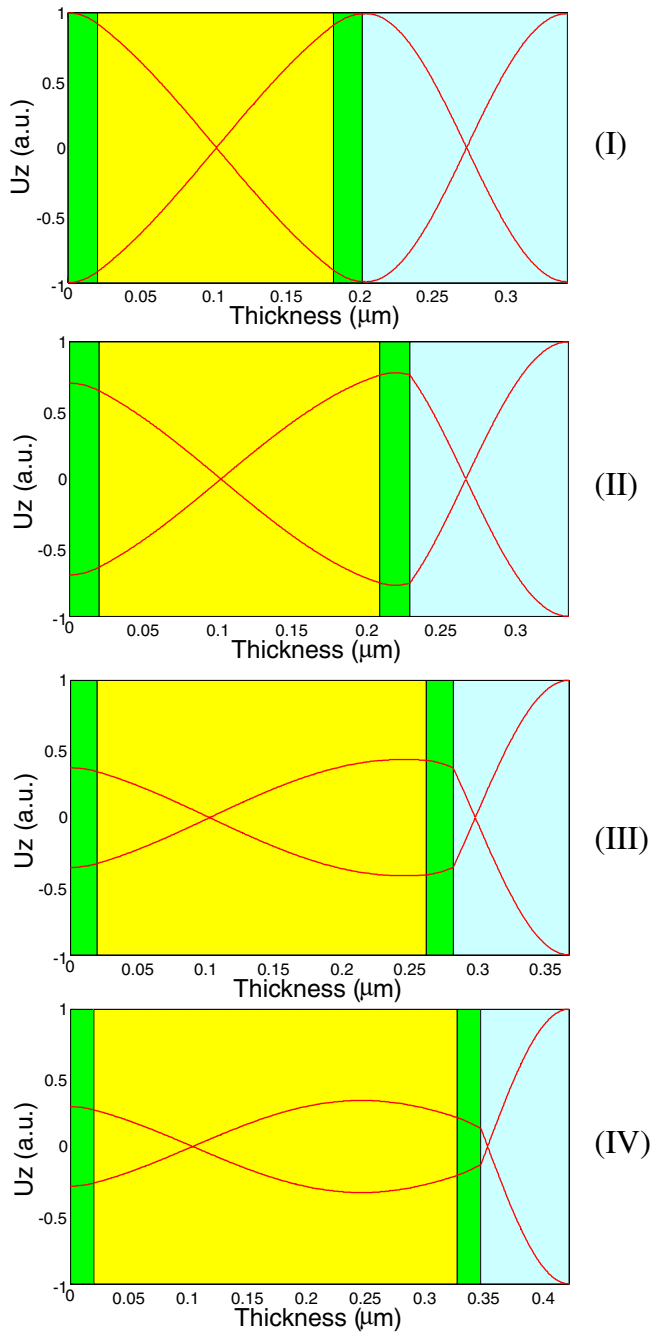


Figure 11. Calculated relative displacement for the second harmonic mode, 20 GHz FBAR consisting of metal/AlN/metal/SiO₂ (from left to right), as described in figure 10. Four sampling points are marked from (I) to (IV) in figure 10. Note that smaller relative displacement corresponds to smaller mass sensitivity.

2.4. Temperature compensation for second harmonic mode FBARs

In the previous sections, we have simulated a second harmonic mode FBAR consisting of Mo/AlN/Mo/SiO₂. By introducing a temperature compensation material (i.e. SiO₂) into the acoustic stack of a resonator (either outside of the metal electrodes or between one of the two electrodes and piezoelectric layer), the temperature stability of the FBAR has been improved to a level comparable to quartz resonators [11,

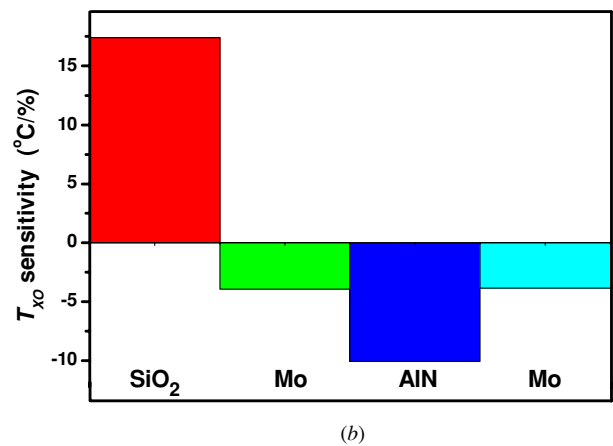
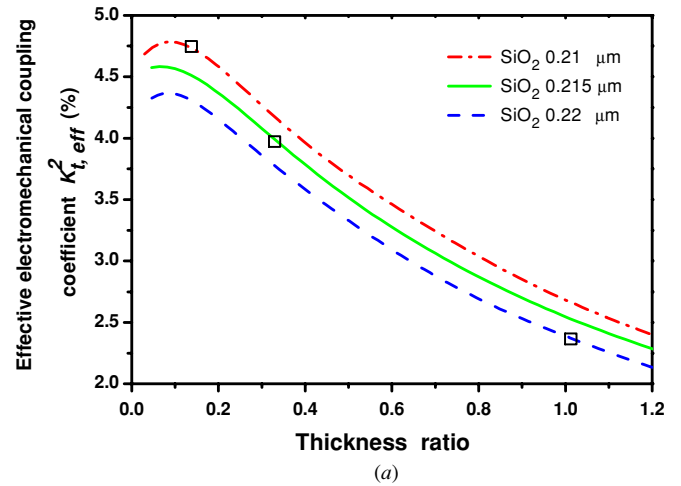


Figure 12. (a) Simulated electromechanical coupling coefficients (of a fundamental mode, 5 GHz FBAR consisting of Mo/AlN/Mo/SiO₂ with SiO₂ thickness as a parameter) versus Mo to AlN thickness ratio. (b) T_{XO} sensitivity in each layer in one representative resonator when the SiO₂ layer is 0.21 μm thick.

[12]. A Mason model based on transmission-line formalism is used to predict the frequency–temperature ($f-T$) sensitivity of the FBAR at 5 GHz using material parameters in [11]. Once the linear drift term has been eliminated from the $f-T$ sensitivity curve, one can define the residual parabolic dependence with two variables; the quadratic term α (typically $-22 \text{ ppb } ^\circ\text{C}^{-2}$) and the temperature crossover point (T_{XO}) where the derivative of the frequency versus temperature is flat. The thickness non-uniformity of each composite layer not only causes the frequency variation, but also affects T_{XO} . We assume 1% thickness deviation of each layer, calculate the T_{XO} shift in figures 12(b) and 13(b), and define it as the T_{XO} sensitivity ($^\circ\text{C}/\%$). Figures 12(a) and 13(a) show the calculated dependence of the electromechanical coupling on the thickness ratio of SiO₂ to AlN for the fundamental mode FBAR at 5 GHz when SiO₂ is positioned outside and inside the electrode, respectively. A thinner SiO₂ layer is needed to achieve the same compensation effect when the SiO₂ layer is placed closer to the high-stress region inside the acoustic stack. Arranging the SiO₂ layer between the two electrodes also produces $\sim 15\%$ higher $K_{t,\text{eff}}^2$, which is desirable for many filter/duplexer applications. Similarly,

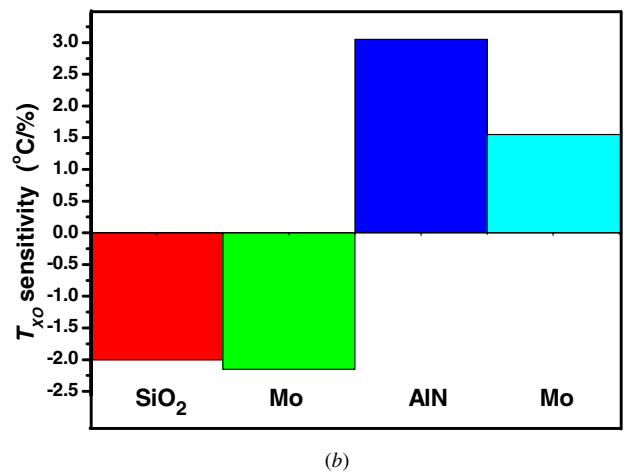
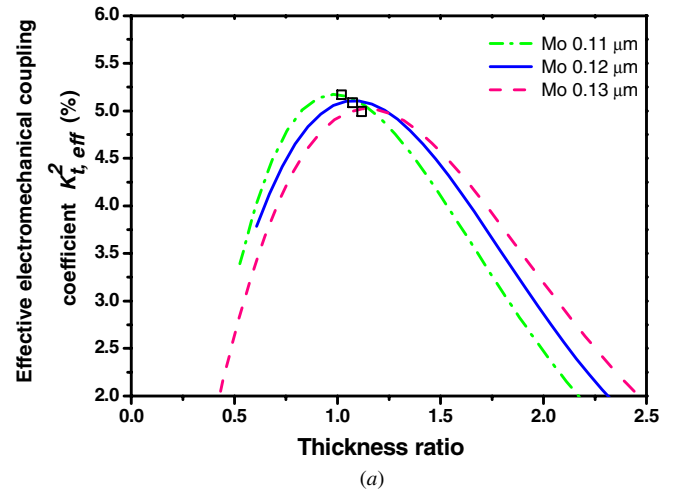
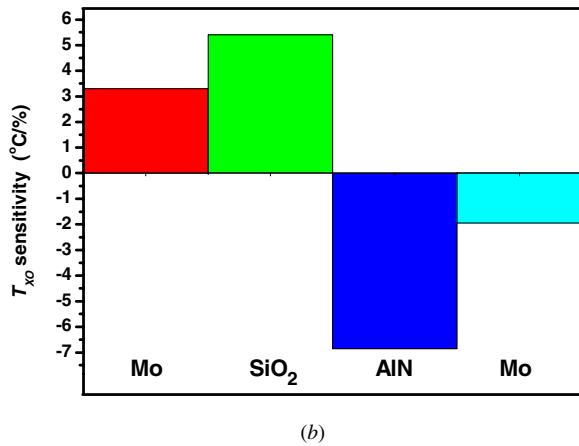
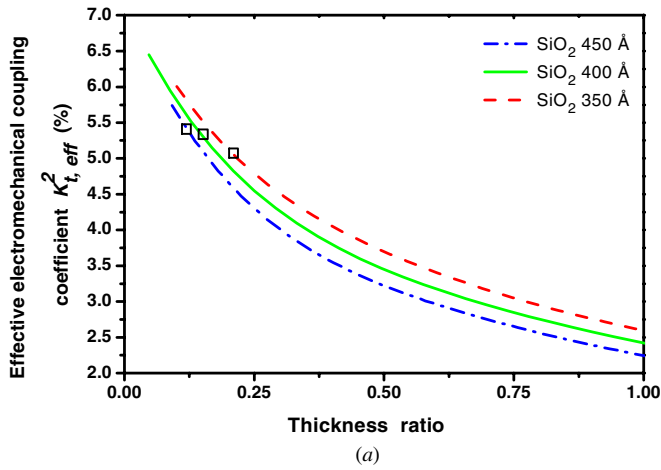


Figure 13. (a) Simulated electromechanical coupling coefficients (of fundamental mode, 5 GHz FBAR consisting of Mo/SiO₂/Mo with SiO₂ thickness as a parameter) versus Mo to AlN thickness ratio. (b) T_{XO} sensitivity in each layer in one representative resonator when the SiO₂ layer is 450 Å thick.

Figure 14. (a) Simulated electromechanical coupling coefficients (second harmonic mode, 5 GHz FBAR consisting of Mo/SiO₂/Mo/SiO₂ with Mo electrode thickness as a parameter) versus SiO₂ to AlN thickness ratio. (b) T_{XO} sensitivity analysis in each layer in one representative resonator when the Mo layer is 0.11 μm.

Table 3. Comparison of $K_{t,eff}^2$ and layer thicknesses of the fundamental and second harmonic mode, temperature compensated FBARs at 5 GHz (unit: Å).

Fundamental mode		Second harmonic mode	
$K_{t,eff}^2 = 4.7\%$	$K_{t,eff}^2 = 5.39\%$	$K_{t,eff}^2 = 5.16\%$	$K_{t,eff}^2 = 4.42\%$
2100 (SiO ₂)	710 (Mo)	5600 (SiO ₂)	1600 (Mo)
790 (Mo)	450 (SiO ₂)	1100 (Mo)	3440 (SiO ₂)
4720 (AlN)	5770 (AlN)	5200 (AlN)	7080 (AlN)
790 (Mo)	710 (Mo)	1100 (Mo)	1600 (Mo)

figures 14 and 15 show the calculated dependence of the electromechanical coupling on the thickness ratio of SiO₂ to AlN and T_{XO} sensitivity for the second harmonic mode FBAR at 5 GHz, when SiO₂ is positioned outside and inside the electrode, respectively. In figures 12(a)–15(a) are marked the points where $K_{t,eff}^2$ is maximized and T_{XO} is around 25 °C (±5 °C error). Comparison of $K_{t,eff}^2$ and layer thicknesses between the fundamental and second harmonic mode temperature-compensated FBARs is summarized in table 3. The overall T_{XO} sensitivity in the second harmonic mode case is at least two to three times less than that in the fundamental mode,

while the maximum $K_{t,eff}^2$ (5.39% versus 5.16%) is very close. Moreover, the SiO₂ in the second harmonic mode is not as thin as that for the fundamental mode. In general, the second harmonic mode FBAR requires less stringent manufacturing process control than the fundamental mode FBAR, for timing and reference clock generation applications, especially when the frequency is beyond 10 GHz.

3. Experimental results

For experimental verification, we have fabricated membrane-type FBARs with the thickness of the bottom and top Al electrodes fixed at 0.15 μm and 0.1 μm, respectively. The FBARs are fabricated on 3 inch, single-side polished silicon wafers. As shown in figure 1(a), the FBARs are built on a LPCVD Si_xN_y diaphragm formed by bulk micromaching (KOH etching) of silicon from the wafer backside. Five variations of FBARs have been fabricated and measured. The FBAR active area is 80 × 80 μm² as this size gives the best impedance match to a 50 Ω line.

Table 4. Measured structure parameters and performances of the fabricated FBARs ($\text{Si}_x\text{N}_y/\text{Al}/\text{ZnO}/\text{Al}$).

No.	Si_xN_y thickness (μm)	ZnO thickness (μm)	ZnO/ Si_xN_y thickness ratio	Resonance frequency (GHz)		$K_{t,\text{eff}}^2$ (%)
				f_s (series)	f_p (parallel)	
FBAR-1	0.2	0.88	4.4	4.983 50	4.999 54	0.79
FBAR-2	0.3	0.78	2.6	4.966 53	5.014 51	2.35
FBAR-3	0.6	0.62	1.08	5.036 56	5.117 10	3.88
FBAR-4	1.1	0.48	0.43	5.014 56	5.070 10	2.73
FBAR-5	1.2	0.42	0.35	4.872 15	4.900 87	1.45

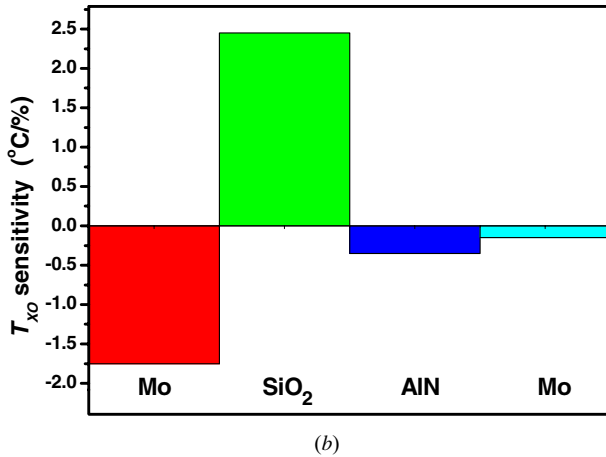
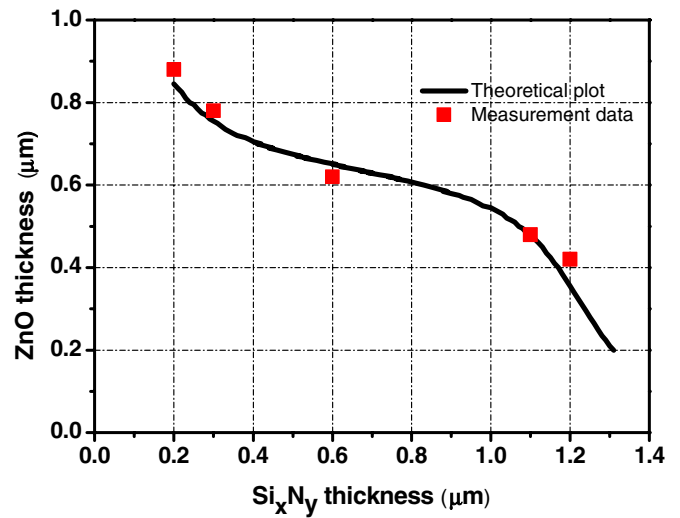
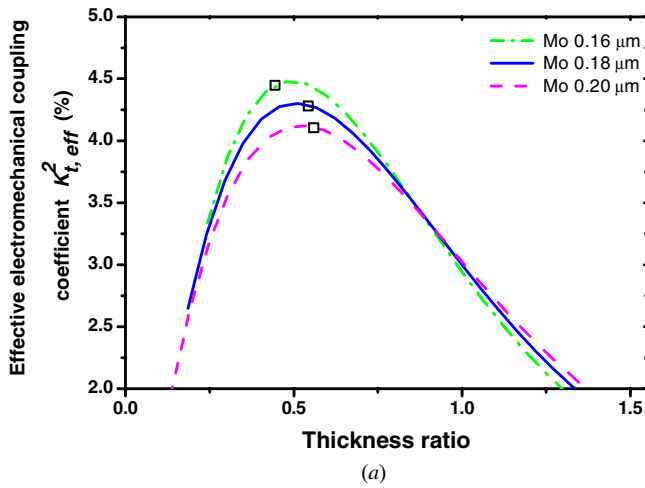


Figure 15. (a) Simulated electromechanical coupling coefficients (second harmonic mode, 5 GHz FBAR consisting of Mo/AlN/SiO₂/Mo with Mo electrode thickness as a parameter) versus SiO₂ to AlN thickness ratio. (b) T_{XO} sensitivity in each layer in one representative resonator when the Mo layer is 0.16 μm .

As summarized in table 4, the ZnO thickness is varied from 0.42 to 0.88 μm , while the ratio of the ZnO thickness to Si_xN_y thickness is varied from 0.35 to 4.4, to make the second harmonic mode resonant frequency fall between 4.87 and 5.03 GHz. The thicknesses of ZnO and Si_xN_y are measured with a profilometer over patterned steps. The effective coupling coefficient $K_{t,\text{eff}}^2$ of the FBAR is calculated from the measured series and parallel frequencies.

The fabricated FBARs are tested in a probe station at atmospheric pressure with G-S-G 150 pitch probes from Cascade. The calibration is carried out with an

Figure 16. ZnO thickness versus Si_xN_y thickness for an FBAR ($\text{Si}_x\text{N}_y/\text{Al}/\text{ZnO}/\text{Al}$) for constant second harmonic mode resonant frequency at 5 GHz.

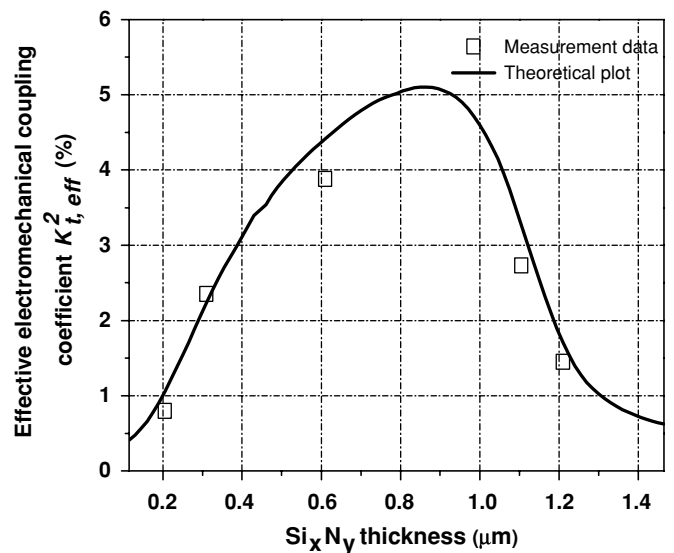


Figure 17. Measured and calculated plots of the effective electromechanical coupling coefficient ($K_{t,\text{eff}}^2$) as a function of the support layer (Si_xN_y) thickness for the four-layer FBAR ($\text{Si}_x\text{N}_y/\text{Al}/\text{ZnO}/\text{Al}$).

impedance standard substrate and short-open-load (SOL) method. The reflection coefficient, S_{11} , of each FBAR is measured by a network analyzer (HP 8753D) and is used to calculate the impedance of the FBAR in Matlab via $Z_{in} = 50(1+S_{11})/(1-S_{11})$.

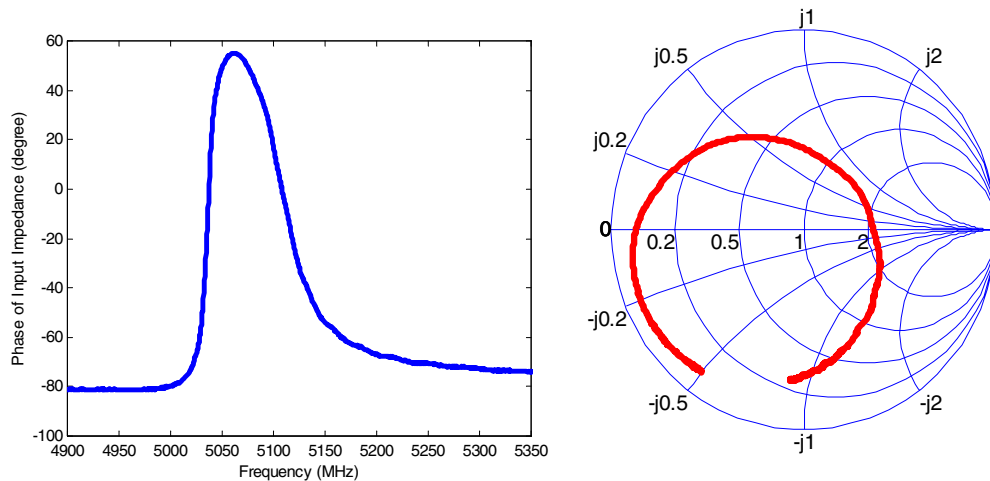


Figure 18. Measured second harmonic mode response of the FBAR composed of $0.6\ \mu\text{m}$ LPCVD- Si_xN_y / $0.15\ \mu\text{m}$ Al/ $0.62\ \mu\text{m}$ -ZnO/ $0.1\ \mu\text{m}$ Al: phase of the impedance (left) and Smith-chart impedance (right).

Mason's model is also used to choose the ZnO thickness while varying the thickness ratio between the ZnO and support layers to keep the second harmonic mode resonant frequency constant at 5 GHz, and figure 16 shows the measured results and theoretical predictions. As shown in figure 17 (that plots both the measured and simulated data), the thickness of the non-piezoelectric layer (i.e. Si_xN_y) affects the $K_{t,\text{eff}}^2$ of the four-layer FBAR. Experimentally, we have so far obtained the best $K_{t,\text{eff}}^2$ of 3.88% with an unloaded Q of 680 near 5 GHz, a second harmonic mode resonant frequency of the FBAR composed of $0.6\ \mu\text{m}$ Si_xN_y / $0.15\ \mu\text{m}$ Al/ $0.62\ \mu\text{m}$ ZnO/ $0.1\ \mu\text{m}$ Al, as shown in figure 18.

4. Summary

In this paper, the impedance equations for both the four-layer (metal/piezoelectric film/metal/non-piezoelectric film) and three-layer (thin metal/piezoelectric film/thick metal) FBARs are derived from Mason's model to analyze the second harmonic mode response of the FBAR, especially the influences of the non-piezoelectric layer on the resonator characteristics. The dependences of $K_{t,\text{eff}}^2$ and mass sensitivity on various parameters have been studied and correlated with stress and displacement distributions within the composite structure. The advantages of mass/trimming sensitivity together with relaxed fabrication tolerances of the second harmonic mode over the fundamental one for the temperature compensated FBAR are identified and discussed. We have fabricated and tested membrane-type, ZnO-based 5 GHz FBARs on an LPCVD Si_xN_y diaphragm, and obtained good agreement between simulation and experimental results.

Acknowledgment

This material is partially based upon work supported by Defense Advanced Research Projects Agency (DARPA) under contract no N66001-02-1-8918.

References

- [1] Ruby R C, Bradley P, Oshmyansky Y, Chien A and Larson J D III 2001 Thin film bulk acoustic resonators (FBAR) for wireless applications *IEEE Ultrasonics Symp.* pp 813–21
- [2] Larson J D III and Oshmyansky Y 2002 Measurement of effective k_t^2 , Q , R_p , R_s vs. temperature for Mo/AlN FBAR resonators *IEEE Ultrasonics Symp.* pp 939–43
- [3] Yokoyama T, Hara M, Ueda M and Satoh Y 2008 K-band ladder filters employing air-gap type thin film bulk acoustic resonators *IEEE Ultrasonics Symp.* pp 598–601
- [4] Hara M, Yokoyama T, Sakashita T, Ueda M and Satoh Y 2009 A study of the bulk acoustic wave resonator filters in several ten GHz band *IEEE Ultrasonics Symp.* pp 851–4
- [5] Zhang H and Kim E S 2005 Micromachined acoustic resonant mass sensor *J. Microelectromech. Syst.* **14** 699–706
- [6] Hashimoto K-Y 2009 *RF Bulk Acoustic Wave Filters for Communication* (Boston, MA: Artech House Publishers)
- [7] Zhang Y, Wang Z, David J and Cheeke N 2003 Resonant spectrum method to characterize piezoelectric films in composite resonators *IEEE Trans. Ultrason. Ferroelectr. Freq. Control.* **50** 321–33
- [8] Johnston M L, Kymissis I and Shepard K L 2010 FBAR-CMOS oscillator array for mass-sensing applications *IEEE Sensors J.* **10** 1042–7
- [9] Josse F, Lee Y, Martin S J and Cernosek R W 1998 Analysis of the radial dependence of mass sensitivity for modified-electrode quartz crystal resonators *Anal. Chem.* **70** 237–47
- [10] Wingqvist G, Yantchev V and Katardjiev I 2008 Mass sensitivity of multilayer thin film resonant BAW sensors *Sensors Actuators A* **148** 88–95
- [11] Pang W, Ruby R C, Parker R, Fisher P W, Unkrich M A and Larson J D 2008 A temperature-stable film bulk acoustic wave oscillator *IEEE Electron. Device Lett.* **29** 315–8
- [12] Rai S, Su Y, Pang W, Ruby R and Otis B 2010 A digitally compensated 1.5 GHz CMOS/FBAR frequency reference *IEEE Trans. Ultrason. Ferroelectr. Freq. Control.* **57** 552–61